RESEARCH ARTICLE | APRIL 15 2025

Dissipation-induced nonreciprocal second-order sideband generation in cavity magnonics

Xiao-Hu Lu ; Bao Wang ; Hao Xiong

J. Appl. Phys. 137, 153902 (2025)
https://doi.org/10.1063/5.0262946

Journal of Applied Physics ARTICLE pubs.aip.org/aip/jap

Dissipation-induced nonreciprocal second-order sideband generation in cavity magnonics

Cite as: J. Appl. Phys. **137**, 153902 (2025); doi: 10.1063/5.0262946
Submitted: 3 February 2025 · Accepted: 27 March 2025 ·
Published Online: 15 April 2025

Xiao-Hu Lu,[1] Bao Wang,[1,a)] and Hao Xiong[2,a)]

AFFILIATIONS

[1]Academy for Electronic Information Discipline Studies, Nanyang Institute of Technology, Nanyang 473004, China
[2]School of Physics, Huazhong University of Science and Technology, Wuhan 430074, China

[a)]**Authors to whom correspondence should be addressed:** baowang@hust.edu.cn and haoxiong@hust.edu.cn

ABSTRACT

Dissipative coupling generally results in complex effective spin–photon interactions, which have significant applications in nonreciprocal transport and enhanced sensing technologies. In this paper, we consider the cooperative effect of coherent and dissipative magnon–photon couplings in an open cavity magnonical system. By enhancing the magnon Kerr nonlinearity with an additional microwave driving field, magnon-induced nonlinear phenomena such as bistability and second-order sideband generation (SSG) can be obtained. By continuously adjusting the ratio of dissipative to coherent coupling strengths, nonreciprocal SSG is observed near the zero-damping condition. Furthermore, the results show that the isolation ratio (the efficiency of the nonreciprocal SSG) can reach up to 82 dB. In addition, increasing the power of the microwave driving field broadens the control range of the dissipative coupling strength, within which the isolation ratio remains above 10 dB. These findings have potential implications for high-precision measurement and on-chip manipulation of light propagation.

I. INTRODUCTION

Cavity magnonics[1–3] have become an important platform for exploring the interaction between microwave photons and magnons. Magnons are quantized spin waves that can be obtained in ferromagnetic materials such as yttrium iron garnet (YIG). Based on YIG spheres, significant progress has been made in the coherent coupling of magnons to various modes, including microwave photons,[4–7] optical photons,[8–10] phonons,[11–13] superconducting qubits,[14,15] and skyrmions.[16,17] Among them, the cavity magnonical system has achieved some remarkable results in theory and experiment, such as the preparation of quantum states,[12,18] ground state cooling,[19,20] quantum memories,[21] and transducers.[22] In particular, magnon-induced nonlinear phenomena have also been widely discussed, such as magnon-induced transparency/absorption[23,24] and slow light,[25] Kerr effect,[26,27] bistability,[28–30] and higher-order sidebands.[31,32]

Recently, dissipative coupling that requires the imaginary coupling constant between two modes has drawn considerable attention due to its important applications to nonreciprocal transport and enhanced sensing, such as chiral mode switching[33] and highly sensitive optical gyroscope for the precision measurement of rotations.[34] The dissipative coupling that originates from reservoir-mediated damping has also been discovered in cavity magnonics,[35] for example, the dissipative magnon–photon coupling[36,37] and the dissipative magnon–magnon coupling.[38,39] Both coherent coupling and dissipative coupling have now been achieved in cavity magnonical systems consisting of a cross-line microwave circuit and a YIG sphere where the interaction between a magnon mode and a cavity mode is mediated by the standing photons and the traveling photons. Based on the cooperative effect of coherent and dissipative magnon–photon couplings, many interesting and important phenomena such as nonreciprocity and unidirectional invisibility for microwave propagation,[40–42] nonreciprocal magnon blockade,[43] nonreciprocal magnon entanglement,[44] enhanced sensing of weak anharmonicities,[45] exceptional-point-engineered optical transmission,[46,47] and observation of unconventional singularity[48] have been reported. In addition, the dissipative coupling can be utilized to achieve anti-parity-time-symmetry (anti-PTS) cavity magnonic systems, which provides a new tool to study non-Hermitian physics of cavity magnonics. Furthermore, some important and useful nonlinear effects have been explored such

as dissipative-coupling-mediated magnon bistability[49,50] and high-order sidebands.[51] The nonlinear phenomena can offer insight into the understanding of the magnon–photon interaction and promote the development of non-Hermitian magnonics.

It is worth mentioning that second-order sideband generation (SSG) in optomechanical systems[52–55] and cavity magnonic systems[56–58] is a typical nonlinear phenomenon, which plays an important role in exploring the nonlinear interactions between photons, phonons, and magnons. Studies have shown that the SSG mainly comes from the intrinsic nonlinearity of the system, which can be divided into three categories: optomechanical nonlinear interaction, magnomechanical nonlinear interaction, and Kerr nonlinearity. Different from optomechanically/magnomechanically induced transparency,[59,60] the SSG is a two-photon conversion process excited by the strong control field. Generally, the SSG can be obtained by preserving high-order minima of the nonlinear interaction terms, but it is relatively inefficient. In order to further explore the nonlinear interactions between photons, phonons, and magnons, some methods have been proposed to enhance SSG, including the atom-cavity coupling system,[61,62] nonlinear Kerr medium-coupled optomechanical system[63] or PT-symmetric optical cavities,[64] PT-symmetric optomechanical systems,[65,66] single quantum dot cavities-coupled PT-symmetric optical cavities,[67] and hybrid cavity–magnon optomechanical system.[68] Additionally, nonreciprocal phenomena based on SSG have been discussed. Nonreciprocal SSG has been realized in spinning optomechanical[69] and magnomechanical[70] systems via the Sagnac effect, as well as in a cavity magnonics system[71] with two microwave cavities and a YIG sphere, utilizing magnon Kerr nonlinearity.

Inspired by recent experimental and theoretical work,[40,72–75] we propose a scheme to realize nonreciprocal SSG in an open cavity magnonical system. In the work, the cavity magnonical system consists of a cross-line microwave circuit and a YIG sphere, where coherent coupling and dissipative magnon–photon coupling are considered simultaneously. Based on the magnon Kerr nonlinearity, the bistable behavior of the magnon population can be regulated by the microwave driving field. The results show that the dissipative coupling strength can regulate the efficiency of the SSG. Compared to the SSG in the cavity magnonical system considering only coherent magnon–photon coupling, our system can enhance the efficiency of SSG by about 40 times. In particular, the efficiency of SSG can be significantly enhanced under zero dissipation conditions (ZDCs). By appropriately adjusting the ratio of dissipative to coherent coupling strengths, nonreciprocal SSG can be realized under ZDC. In addition, the efficiency of the nonreciprocal SSG can be regulated by the microwave driving field. Selecting a larger microwave driving field power can broaden the regulation range of the dissipative coupling strength and enable the nonreciprocal SSG to be realized.

II. PHYSICAL SETUP AND DYNAMICAL EQUATION

We consider an open cavity magnonical system consisting of a cross-line microwave circuit and a yttrium iron garnet (YIG) sphere with a diameter of 1 mm, as shown in Fig. 1(a). This physical model contains coherent and dissipative magnon–photon coupling.[40] Specifically, the magnon mode in the YIG sphere is

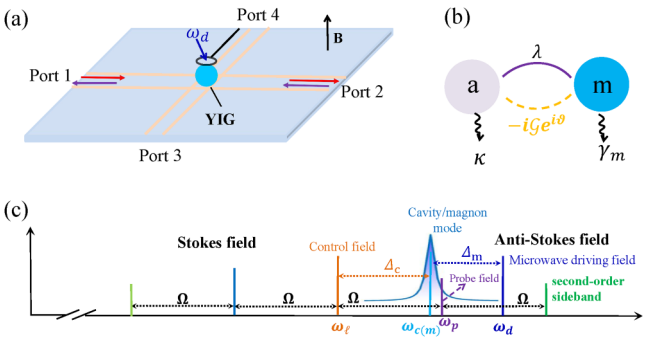

FIG. 1. (a) Schematic diagram of the cavity magnonical system, which consists of a cross-line circuit and a YIG sphere. An additional microwave driving field (with frequency ω_d) is introduced to enhance the magnon Kerr nonlinearity. A ring coil, positioned above the YIG sphere, enables precise control over the decay rate of the magnon mode. In addition, the cavity mode formed between ports 3 and 4 supports both coherent and dissipative interactions with the magnon mode. The spectroscopy is measured with a vector network analyzer through ports 1 and 2. (b) Schematic diagram of the coherent and dissipative couplings among the cavity mode and the magnon mode with the coupling strengths λ and $-i\mathcal{G}e^{i\vartheta}$, respectively. κ and γ_m are, respectively, the damping rates of the cavity and magnon modes. (c) Frequency spectrogram of the cavity magnonical system.

coupled to the standing cavity mode with the coherent magnon–photon coupling strength λ via the magnetic dipole interaction. In addition, the magnon mode interacts with the cavity mode through the dissipative magnon–photon coupling strength $\mathcal{G}$, while the traveling wave contributes to the external damping of both the cavity mode and the magnon mode. The traveling wave induces magnon dissipation by radiating energy into the open environment, distinct from the intrinsic dissipation of magnons and photons.[76] The radiative broadening of the magnon linewidth at and off cavity resonance enables the determination of coherent and dissipative coupling strengths, respectively. The interaction between the magnons and the standing or traveling cavity modes can be tuned by adjusting the torque exerted by the microwave magnetic field on the magnetization or by adjusting the position of YIG sphere. A static magnetic field $\mathbf{B}_z = B\mathbf{e}_z$ in the z direction can magnetize the YIG sphere to form the magnon modes. The Hamiltonian of the uniformly magnetized YIG sphere is given by

$$\mathrm{H}_m = -\int_{V_m} \mathbf{M}\cdot\mathbf{B}_z d\tau - \frac{\mu_0}{2}\int_{V_m} \mathbf{M}\cdot\mathbf{H}_{an} d\tau, \tag{1}$$

where $\mathbf{M} = \hbar\gamma\mathbf{S}/V_m \equiv (M_x, M_y, M_z)$ is the magnetization of the YIG sphere, γ is the gyromagnetic ratio, V_m is the volume of the YIG sphere and μ_0 is the vacuum permeability. $\mathbf{S} \equiv (S_x, S_y, S_z)$ denotes the collective spin operator. Herein, setting the 100 crystallographic axis of the YIG sphere in the z direction, which is aligned along the direction of the applied static magnetic field. Subsequently, the anisotropic field $\mathbf{H}_{an}$, arisen from the magnetocrystalline anisotropy in the YIG crystal, is given by $-2K_{an}M_z/M^2\mathbf{e}_z$ with K_{an} and M being the dominant first-order anisotropy constant and the

saturation magnetization, respectively. The Holstein–Primakoff transform states $S_z = S - m^\dagger m$, where S and S_z represent, respectively, the total spin number of the YIG sphere, and the z component of the spin operator, and $m\,(m^\dagger)$ is the annihilation (creation) operator of the magnon mode. Then, the Hamiltonian in Eq. (1) can be rewritten as

$$\begin{aligned} \mathrm{H}_m/\hbar &= -B_z M_z V_m + \frac{\mu_0 K_{an} M_z^2}{M^2} V_m = -\gamma B_z S_z + \frac{\mu_0 K_{an}\gamma^2}{M^2 V_m} S_z^2 \\ &= \omega_m m^\dagger m + K m^\dagger m m^\dagger m, \end{aligned} \tag{2}$$

where $\omega_m = \gamma B_z - 2\mu_0 K_{an}\gamma^2 S/(M^2 V_m)$ is the analytical expression of the frequency of the magnon mode, and $K = \mu_0 K_{an}\gamma^2/(M^2 V_m)$ is the Kerr nonlinear coefficient. Excitingly, Eq. (2) is the starting point of our following discussion. Additionally, we consider that the cavity magnonical system is driven by a strong control field and a relatively weak probe field with frequencies ω_ℓ, ω_p and amplitudes ε_ℓ, ε_p, respectively. To enhance the strength of magnon Kerr nonlinearity K, a microwave driving field with frequency ω_d and amplitude ε_d is applied to the YIG sphere. In a rotating frame of the control field frequency ω_ℓ, the total Hamiltonian reads

$$\begin{aligned} \mathscr{H} &= \hbar\Delta_c \hat{a}^\dagger \hat{a} + \hbar\Delta_m \hat{m}^\dagger \hat{m} + \hbar K \hat{m}^\dagger \hat{m} \hat{m}^\dagger \hat{m} \\ &\quad + \hbar(\lambda - i\mathscr{G}e^{i\vartheta})(\hat{a}^\dagger \hat{m} + \hat{m}^\dagger \hat{a}) \\ &\quad + i\hbar\sqrt{\kappa/2}\varepsilon_\ell(\hat{a}^\dagger - \hat{a}) + i\hbar\sqrt{\kappa/2}\varepsilon_p(\hat{a}^\dagger e^{-i\Omega t} - \hat{a}e^{i\Omega t}) \\ &\quad + i\hbar\sqrt{\gamma_m/2}\varepsilon_d(\hat{m}^\dagger e^{-i\Delta_m t} - \hat{m}e^{i\Delta_m t}), \end{aligned} \tag{3}$$

which is transformed into the rotation coordinate by unitary transformation $U(t) = \exp[-i\omega_\ell(\hat{a}^\dagger \hat{a} + \hat{m}^\dagger \hat{m})t]$. $\hat{a}\,(\hat{a}^\dagger)$ is the annihilation (creation) operator of the cavity mode. The propagation direction is determined by the phase ϑ, which is 0 and π for microwaves loaded from ports 1 and 2, respectively. $\Delta_{c(m)} = \omega_{c(m)} - \omega_\ell$ denotes the detuning from the cavity (magnon) mode, and $\Omega = \omega_p - \omega_\ell$ indicates the beat frequency between the control field and the probe field. The normalized amplitudes of the driving fields are $\varepsilon_i = \sqrt{P_i/(\hbar\omega_i)}\,(i = \ell, p, d)$ with P_ℓ, P_p, P_d being the powers of the control, probe, and microwave fields, respectively.

Based on the Hamiltonian in Eq. (3), the system dynamics can be well described by the Heisenberg–Langevin equations ($\dot{\rho} = \frac{i}{\hbar}[H, \rho]$) including the dissipation,

$$\begin{aligned} \frac{da}{dt} &= -i\Delta_c a - \kappa/2 a - i(\lambda - i\mathscr{G}e^{i\vartheta})m + \sqrt{\kappa/2}(\varepsilon_\ell + \varepsilon_p e^{-i\Omega t}), \\ \frac{dm}{dt} &= -i\Delta_m m - \gamma_m/2 m - i(\lambda - i\mathscr{G}e^{i\vartheta})a - i(2Km^* m + K)m \\ &\quad + \sqrt{\gamma_m/2}\varepsilon_d e^{-i\Delta_m t}, \end{aligned} \tag{4}$$

where $\kappa\,(\gamma_m)$ is the decay rate of the cavity (magnon) mode. All operators are reduced to their expectation values in the case of considering the mean response of the system, viz., $a = \langle\hat{a}\rangle$, $m = \langle\hat{m}\rangle$, as well as $m^* = \langle\hat{m}^\dagger\rangle$, and the quantum correlations and noise terms can be safely dropped based on the semiclassical approximation. In addition, the mean-field approximation by factorizing averages, i.e., $\langle\hat{m}^\dagger\hat{m}\rangle = m^* m$, is used to deal with the nonlinear term $-i(2Km^* m + K)m$.

Assuming that the control field is much stronger than the probe field, we can employ the perturbation method to solve the evolution equation (4); that is, the solution of Eq. (4) can be written as the sum of the steady-state values and small perturbations. Physically, the strong driving fields, including the control field and the microwave field, provide the steady-state solutions of the cavity magnonical system, and the weak probe field provides the perturbations around the steady states. The perturbations include first-, second-, third-, and higher-order sidebands, which are generated by the parametric frequency conversion arising from the nonlinear interaction. Consequently, the solution can be completely expressed in the following series form:

$$\begin{aligned} a &= A_0 + A_1^+ e^{-i\Omega t} + A_1^- e^{i\Omega t} + A_2^+ e^{-2i\Omega t} + A_2^- e^{2i\Omega t} + \cdots, \\ m &= M_0 + M_1^+ e^{-i\Omega t} + M_1^- e^{i\Omega t} + M_2^+ e^{-2i\Omega t} + M_2^- e^{2i\Omega t} + \cdots, \end{aligned} \tag{5}$$

where A_0 and M_0 are the steady-state solutions of intracavity field and magnon caused by the control field and microwave driving field in the absence of the probe field ($\varepsilon_p = 0$), which shows that the system dynamics will enter into a steady state after a short-time evolution. The frequency components $\pm 2\Omega$ in Eq. (5) are the second-order sideband in a frame rotating with the control field frequency ω_c. In the perturbative regime, the higher-order sidebands, such as third- and four-order sidebands, as well as other higher-order frequency components, are of great weak in contrast to the second-order sideband and are validly ignored.

Setting $dA_0/dt = 0$ and $dM_0/dt = 0$, we can obtain

$$\begin{aligned} A_0 &= \frac{-i(\lambda + i\mathscr{G})M_0 + \sqrt{\kappa/2}\varepsilon_\ell}{i\Delta_c + \kappa/2}, \\ M_0 &= \frac{\varepsilon_d - i(\lambda + i\mathscr{G})A_0}{i\Delta_m + \gamma_m/2 + 2iK|M_0|^2}. \end{aligned} \tag{6}$$

Here, $|A_0|^2$ and $|M_0|^2$ denote, respectively, the steady-state average intracavity photon number and magnon number. According to Eq. (6), we can obtain the following function relationship of $|M_0|^2$:

$$\left[\gamma_m^2/4 + (2K|M_0|^2 + \Delta_m)^2 - (\lambda + i\mathscr{G})^2\mathscr{C}\right]|M_0|^2 = \varepsilon_d^2 + \mathscr{C}\kappa\varepsilon_\ell^2/2, \tag{7}$$

where $\mathscr{C} = (\lambda + i\mathscr{G})^2/(\Delta_c^2 + \kappa^2/4)$. By calculating Eq. (7), in Fig. 2, we display the steady-state magnon number $|M_0|^2$ as a function of power of the microwave driving field P_d for the three different values of the detuning (Δ_m) of the probe field frequency ω_p from the frequency of magnon mode ω_m, that is, $\Delta_m = -0.3$ GHz, $\Delta_m = -0.25$ GHz, $\Delta_m = -0.2$ GHz, respectively, correspond to the blue curve line, the red curve line, and the magenta curve line. As clearly shown in Fig. 2, the magnon number $|M_0|^2$ experiences a bistable behavior of P_d in a certain parameter region, which states that the magnonic response exhibits two different stable states, namely, although $|M_0|^2$ possesses three real roots, but the dashed

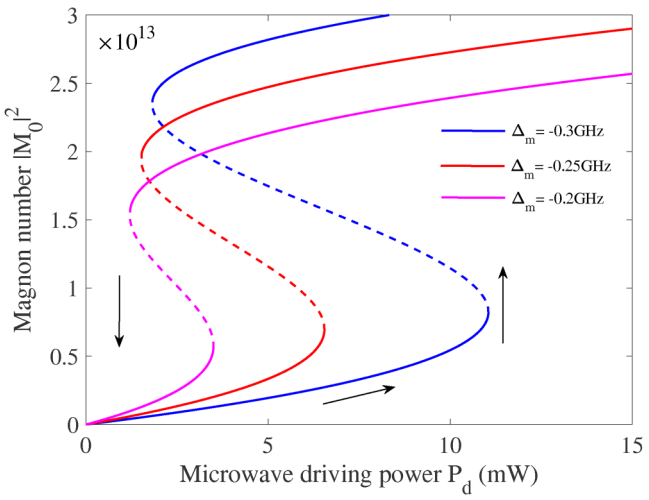

FIG. 2. Magnon bistability as seen through the steady-state magnon number $|M_0|^2$ varied with the power of the microwave driving field P_d for the three different detunings $\Delta_m = -0.3, -0.25, -0.2$ GHz corresponding to blue, red, and magenta curve lines, respectively. The other system parameters are $P_\ell = 0$ W, $\kappa/2\pi = 881.1$ MHz, $\Delta_c = 0.05\kappa$.

lines in Fig. 2 signify the unstable solutions. Note furthermore that the system undergoes from the lower steady state to the upper steady state and the opposite process with increasing and decreasing P_d, which is similar to the hysteresis loop in ferromagnetic materials.

Next, we calculate the amplitude of the SSG analytically to describe the underlying physical process. By substituting the ansatz equations (5) into the Heisenberg–Langevin equation (4), we can obtain

$$\begin{aligned}
(\delta_c - i\Omega)A_1^+ &= -i(\lambda - i\mathcal{G}e^{i\vartheta})M_1^+ + \sqrt{\kappa/2}\varepsilon_p,\\
(\delta_c + i\Omega)A_1^- &= -i(\lambda - i\mathcal{G}e^{i\vartheta})M_1^-,\\
(\delta_c - 2i\Omega)A_2^+ &= -i(\lambda - i\mathcal{G}e^{i\vartheta})M_2^+,\\
(\delta_c + 2i\Omega)A_2^- &= -i(\lambda - i\mathcal{G}e^{i\vartheta})M_2^-,\\
(\delta_m - i\Omega)M_1^+ &= -i(\lambda - i\mathcal{G}e^{i\vartheta})A_1^+ - 2iK|M_0|^2(M_1^-)^*,\\
(\delta_m + i\Omega)M_1^- &= -2iKM_0^2(M_1^+)^* - i(\lambda - i\mathcal{G}e^{i\vartheta})A_1^-,\\
(\delta_m - 2i\Omega)M_2^+ &= -2iK[M_0^*(M_1^+)^2 + M_0^2(M_2^-)^*\\
&\quad + 2M_0M_1^+(M_1^-)^*] - i(\lambda - i\mathcal{G}e^{i\vartheta})A_2^+,\\
(\delta_m + 2i\Omega)M_2^- &= -2iK[M_0^*(M_1^-)^2 + M_0^2(M_2^+)^*\\
&\quad + 2M_0M_1^-(M_1^+)^*] - i(\lambda - i\mathcal{G}e^{i\vartheta})A_2^-,
\end{aligned} \tag{8}$$

where $\delta_c = i\Delta_c + \kappa/2$, $\delta_m = i\Delta_m + \gamma_m/2 + 4iK|M_0|^2$. It is worth noting that, according to (8), the physical mechanism of the SSG is demonstrated clearly. That is, the control field with frequency ω_ℓ and the probe field with frequency ω_p are converted into second-order sideband via anti-Stokes scattering ($2\omega_p \to \omega_\ell + \omega_2$, $\omega_2 = \omega_\ell + 2\Omega$), which can be illustrated by $-2iK\left[-2iKM_0^*(M_1^+)^2 + M_0M_1^+(M_1^-)^*\right]$ resulting from the Kerr nonlinearity. By solving for the algebraic equation (8), we can derive the analytical expressions of the amplitudes of first-order sideband generation (FSG) and SSG in the cavity magnonics, yielding

$$\begin{aligned}
A_1^+ &= \frac{i(\lambda - i\mathcal{G}e^{i\vartheta})M_1^+ - \sqrt{\kappa/2}\varepsilon_p}{i\Omega - i\Delta_c - \kappa/2},\\
A_2^+ &= \frac{i(\lambda - i\mathcal{G}e^{i\vartheta})M_2^+}{2i\Omega - i\Delta_c - \kappa/2},\\
M_1^+ &= \frac{i(\lambda - i\mathcal{G}e^{i\vartheta})\sqrt{\kappa/2}\varepsilon_p\varpi(\Omega)^*}{[i\Omega - (i\Delta_c + \kappa/2)][\varpi(-\Omega)\varpi(\Omega)^* - 4K^2|M_0|^4]},\\
M_2^+ &= \frac{(\tau(\Omega) + \phi(\Omega))(M_1^+)^2}{(\varpi(-2\Omega)\varpi(2\Omega)^* - 4K^2|M_0|^4)(\varpi(\Omega)^*)^2},
\end{aligned} \tag{9}$$

with

$$\begin{aligned}
\varpi(x) &= i\Delta_m + \gamma_m/2 + 4iK|M_0|^2\\
&\quad + (\lambda - i\mathcal{G}e^{i\vartheta})^2/(i\Delta_c + \kappa/2 - ix) - ix,\\
\tau(\Omega) &= -16K^4|M_0|^6M_0^* + 8K^2|M_0|^2M_0^*\varpi(2\Omega)^*(\varpi(\Omega)^*)^2,\\
\phi(\Omega) &= 16iK^3|M_0|^4M_0^*\varpi(\Omega)^* - 2iKM_0^*\varpi(2\Omega)^*(\varpi(\Omega)^*)^2.
\end{aligned} \tag{10}$$

Furthermore, performing the standard input–output relation $\mathcal{A}_{out} = \mathcal{A}_{in} - \sqrt{\kappa/2}a$, the amplitudes of the SSG from the output field can be obtained as $-\sqrt{\kappa/2}M_2^+$. To reveal substantially the SSG process, we define the dimensionless and normalized amplitudes $\Pi_1 = \left|1 - \frac{\sqrt{\kappa/2}}{\varepsilon_p}A_1^+\right|$ and $\Pi_2 = \left|\frac{\sqrt{\kappa/2}}{\varepsilon_p}A_2^+\right|$ to describe the efficiency of the upper FSG and SSG. The main parameters we use are from recent experiments,[40,48,77] as follows: $\omega_c/2\pi = 4.724$ GHz, $\lambda/2\pi = 7.9$ MHz, $\mathbb{K}/2\pi = 10^{-10}$ Hz, $\kappa/2\pi = 880$ MHz, $\gamma_m/2\pi = 0.071$ MHz, $\Delta_c = 0.05\,\kappa$, and $\Delta_m = -0.05\,\kappa$.

III. NUMERICAL RESULTS AND DISCUSSION

In order to better understand the physical process of second-order sideband induced by magnon Kerr nonlinearity, in Fig. 3, we plot the efficiency of upper FSG and SSG as a function of detuning of the probe field Ω under different dissipative magnon–photon coupling strength. When $\mathcal{G} = 0$, there is only coherent magnon–photon coupling in the system, and no dissipative magnon–photon coupling. However, when $\mathcal{G} = \lambda$, coherent coupling and dissipative magnon–photon coupling exist simultaneously in the system. As shown in Fig. 3(a), when only coherent magnon–photon coupling is considered, magnon-induced transparency occurs with an efficiency of about 82.51%. When coherent coupling and dissipative coupling are considered simultaneously, the phenomenon of magnon-induced transparency amplification can be realized. Compared with the magnetically induced transparency generated

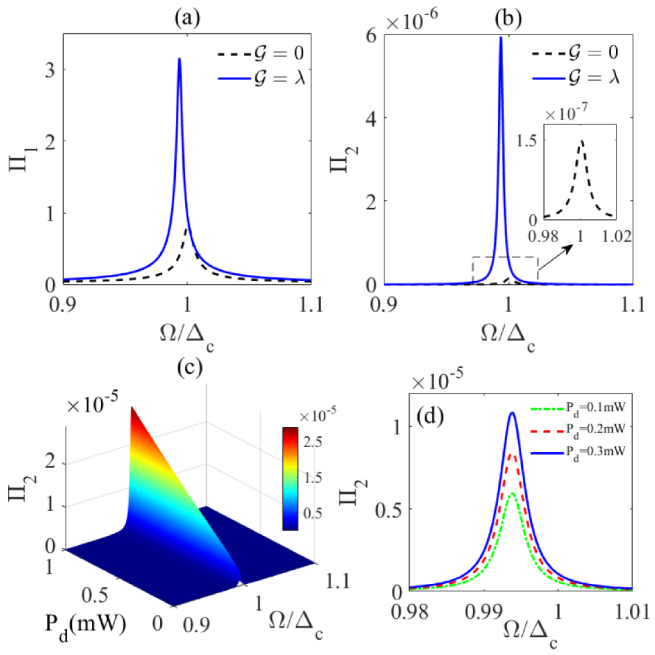

FIG. 3. The efficiency of (a) FSG and (b) SSG as a function of Ω under different dissipative magnon–photon coupling strength $\mathcal{G}$. (a) and (b): Π_1, Π_2 is in the condition of $\mathcal{G}=0$ (black dashed line), $\mathcal{G}=\lambda$ (blue solid line). (c) The efficiency of SSG varied with frequency detuning Ω and the power of the microwave driving field P_d. (d) The efficiency of SSG as a function of Ω under different the power of the microwave driving field P_d. The other system parameters are $\vartheta=\pi$, $P_\ell=0.1$ mW, $P_p=0.005$ mW.

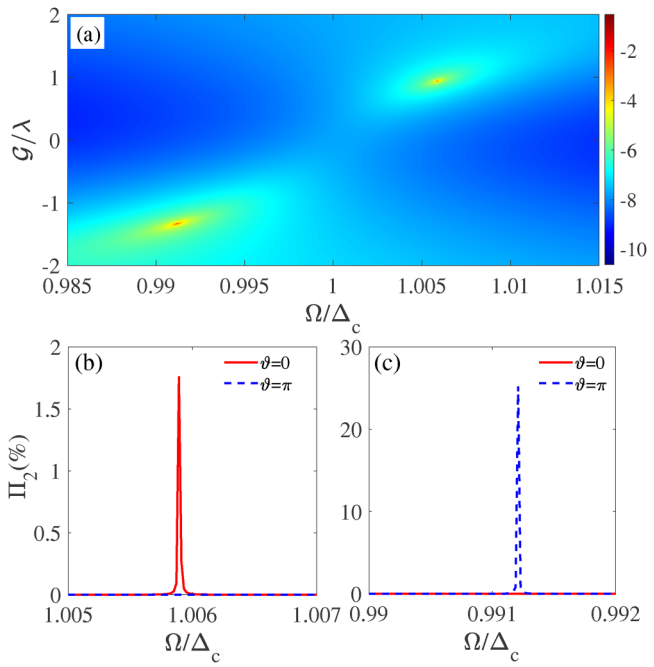

FIG. 4. (a) The efficiency (in logarithmic form) of SSG as a function of frequency detuning Ω and dissipative magnon–photon coupling strengths $\mathcal{G}$. The efficiency of SSG as a function of Ω under (b) $\mathcal{G}/\lambda=0.9395$ and (c) $\mathcal{G}/\lambda=-1.3387$. $\vartheta=0$ and $\vartheta=\pi$ represent the driving fields input from the forward and backward directions, respectively, and $P_\ell=P_d=20\,\mu$W, $P_p=1\,\mu$W.

in other cavity magnonic systems, the system we consider can utilize the dissipative coupling strength to achieve the amplification and broadening of magnetically induced transparency. Furthermore, the efficiency of the SSG is discussed in two cases. In Fig. 3(b), when only coherent coupling is considered, the efficiency of the SSG is only 1.49×10^{-7}. However, when both coherent coupling and dissipative coupling are considered, the efficiency of the SSG is 5.95×10^{-5}, which is about 40 times higher. Generally, the SSG is derived from the upper first-order sideband (the probe field with frequency ω_p), so the stronger upper first-order sideband can enormously increase the power and efficiency of the SSG. The analytical results match well with the analysis of the physical process. In addition, the effect of the microwave driving field on the efficiency of the SSG is discussed. As illustrated in Fig. 3(c), when the detuning ratio Ω/Δ_c remains constant, the efficiency of the SSG exhibits a monotonic increase with increasing microwave driving power P_d. In particular, as shown in Fig. 3(d), both the efficiency and spectral broadening of SSG are enhanced; this trend can be understood in conjunction with the results shown in Fig. 2. Physically, the increase in microwave driving power leads to a nonlinear growth in the magnon number, which, in turn, strengthens the magnon–photon coupling interaction and enhances the magnon Kerr nonlinearity, thereby significantly improving the efficiency of SSG.

In the following, we focus on the effects of the system parameters on the nonreciprocal SSG under the condition that the driving fields input from the forward and backward directions, corresponding to $\vartheta=0$ and π, respectively. As shown in Fig. 4(a), under the condition of $\mathcal{G}>0$, the efficiency of SSG has a maximum value, and the direction of the driving field input is forward, that is, $\vartheta=0$. Similarly, when the direction of the driving field input is backward ($\mathcal{G}<0$), corresponding to $\vartheta=\pi$, the efficiency of SSG reaches a maximum value that is significantly higher than that shown in Fig. 3(b). Theoretically, when $\lambda=\mathcal{G}$, the supermode of two mode coupling will produce two degenerate points, which is defined as the zero dissipation condition (ZDC).[40] Under the ZDC, the imaginary part of the eigenvalue of the effective Hamiltonian becomes zero when the driving term is not considered. The results show that the system can break the time-reversal symmetry of microwave propagation by considering the direction-dependent relative phase between coherent and dissipative magnon–photon coupling. Here, when the correction caused by magnon Kerr nonlinearity is taken into account, the ratio of $\mathcal{G}$ to λ is not strictly equal to 1. As shown in Fig. 4(b), we take $\mathcal{G}/\lambda=0.9395$, and the results show that the efficiency of SSG in the forward transmission is much larger than that in the reverse transmission. Similarly, when $\mathcal{G}/\lambda=-1.3387$, the efficiency of SSG in reverse transmission is much larger than in forward transmission [as shown in

Fig. 4(c)]. This shows that the non-reciprocal transmission of SSG can be achieved under the ZDC.

We define an isolation ratio Φ to describe the efficiency of the nonreciprocal SSG, which can be explicitly given by (the unit of Φ is dB)

$$\Phi = 10 * \log_{10}\left|\frac{\Pi_2(\pi)}{\Pi_2(0)}\right|. \tag{11}$$

Figure 5 discusses the functional relationship between isolation ratio Φ and the dissipative coupling strength under different microwave driving powers. As shown in Fig. 5(a), in the area between the two gray dashed lines, corresponding to $\mathcal{G}/\lambda \in (0.68, 2.48)$, the isolation ratio Φ is greater than 10 dB, and the maximum value is 77.52 dB. Here, the interval with an isolation ratio greater than 10 dB can be regarded as an effective isolation interval, in which nonreciprocal SSG can be achieved by adjusting the ratio of dissipative to coherent coupling strengths. In Fig. 5(b), when the microwave driving field power $P_d = 100\,\mu$W, the isolation ratio Φ is enhanced and the maximum value is 81.62 dB, and, the effective isolation interval increases to $\mathcal{G}/\lambda \in (0.60, 4.49)$. When $P_d = 200\,\mu$W [as shown in Fig. 5(c)], the maximum isolation value is 82.33 dB, and the effective isolation interval ($\mathcal{G}/\lambda \in (0.60, 6.58)$) is about three times that of Fig. 5(a). Furthermore, although the range of dissipative coupling strength regulation can be expanded by continuing to increase the microwave driving field power, the maximum value of the isolation ratio Φ is decreasing. As shown in Fig. 5(d), when $P_d = 400\,\mu$W, within the range of $\mathcal{G}/\lambda \in (0.60, 9.68)$, $\Phi > 10$ dB; but the maximum value of Φ is 82.15 dB, which is smaller than the maximum value of Φ in Fig. 5(c). The results show that there is a suitable microwave driving field power to make the isolation Φ reach the maximum value, and increasing the microwave driving field power within a certain range can ensure the efficiency of nonreciprocal SSG.

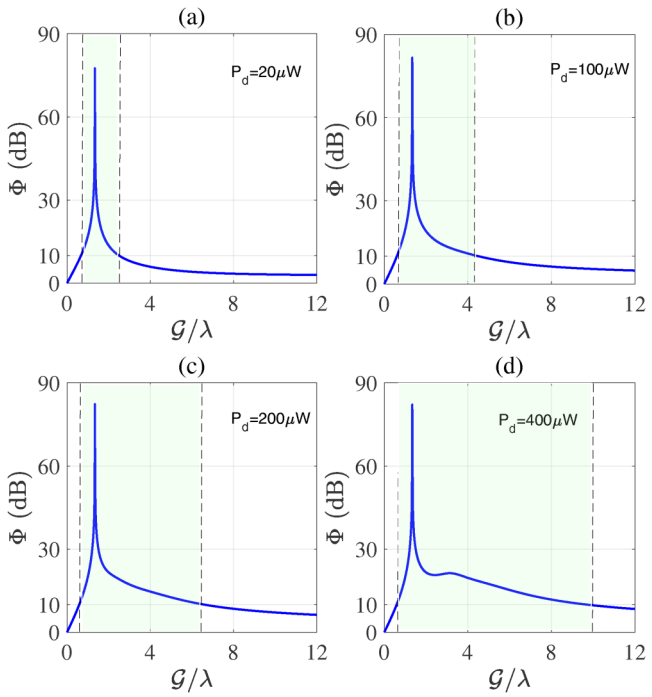

FIG. 5. Calculation results of Φ vary with $\mathcal{G}$ under different powers of the microwave driving field P_d. We use P_d = (a) 20, (b) 100, (c) 200, and (d) 400 μW. The beat frequency $\Omega/\Delta_c = 0.9912$. The other parameters are the same as Fig. 4.

IV. CONCLUSION

In summary, the cavity magnonical system we considered can realize the generation and control of nonreciprocal second-order sidebands. Based on the magnon Kerr nonlinearity, the bistability of the magnons is discussed. The microwave driving field can be used to change the bistability of the magnons, which has potential advantages in controlling the number of magnons. Specifically, the efficiency of SSG is affected by the dissipative magnon–photon coupling strength. Taking the dissipative magnon–photon coupling into account can enhance the efficiency of the SSG. By appropriately tuning the ratio of dissipative to coherent coupling strength, a higher SSG efficiency can be achieved. In addition, the results show that nonreciprocal SSG can be achieved when the system is under the ZDC, and the impact of nonreciprocal SSG can be controlled by the microwave driving field and the dissipative coupling strength. Compared with the hybrid quantum system that realized nonreciprocal SSG in the past, the system we considered has two advantages: First, the structure does not require multiple optical cavities or rotating optical cavities. Second, it relies on the inherent magnon Kerr nonlinearity, which makes it simpler to control the efficiency of the nonreciprocal SSG.

The cavity magnonical system,[40] integrating both coherent and dissipative magnon–photon coupling, can be implemented using a cross-line microwave circuit and a 1 mm YIG sphere. A tunable loop antenna positioned above the YIG sphere enables precise control over the magnon mode's decay rate. It should be noted that when the YIG sphere is coupled to such a planar cavity to form an open cavity magnonical system, the external decay rate of the cavity mode is much larger than its intrinsic decay rate. By adjusting the position of YIG, an anti-PT-symmetric cavity magnonical system[48] with purely dissipative coupling ($\lambda = 0$) was realized, and an unconventional bound state in the continuum (BIC) was observed. It has been experimentally shown that the nonreciprocal device possessing both a high isolation ratio and a broad operating bandwidth can be achieved by locally controlling the radiation damping of the magnon mode.[77] Based on this system, the nonlinear effects of magnons such as magnon frequency combs[72,78] and quantum effects such as magnon blockade[79] and steady-state entanglement[80] can be further explored.

ACKNOWLEDGMENTS

This work was supported by the National Natural Science Foundation of China (NNSFC) (Nos. 12004202 and 12022507); the Natural Science Foundation of Henan Province (No. 242300420652); the Key Research Projects of Higher Education Institutions in Henan

Province (No. 25A140021); and the Interdisciplinary Sciences Project of Nanyang Institute of Technology (No. 24NGJY003).

AUTHOR DECLARATIONS

Conflict of Interest

The authors have no conflicts to disclose.

Author Contributions

Xiao-Hu Lu: Formal analysis (equal); Funding acquisition (equal); Methodology (equal); Software (equal); Validation (equal); Writing – original draft (equal); Writing – review & editing (equal). **Bao Wang:** Conceptualization (equal); Formal analysis (equal); Funding acquisition (equal); Investigation (equal); Methodology (equal); Validation (equal). **Hao Xiong:** Conceptualization (equal); Methodology (equal); Supervision (equal); Validation (equal).

DATA AVAILABILITY

The data that support the findings of this study are available from the corresponding authors upon reasonable request.

REFERENCES

[1]A. V. Chumak, V. Vasyuchka, A. Serga, and B. Hillebrands, "Magnon spintronics," Nat. Phys. **11**, 453–461 (2015).
[2]D. Lachance-Quirion, Y. Tabuchi, A. Gloppe, K. Usami, and Y. Nakamura, "Hybrid quantum systems based on magnonics," Appl. Phys. Express **12**, 070101 (2019).
[3]M. Harder, B. M. Yao, Y. S. Gui, and C.-M. Hu, "Coherent and dissipative cavity magnonics," J. Appl. Phys. **129**, 201101 (2021).
[4]H. Huebl, C. W. Zollitsch, J. Lotze, F. Hocke, M. Greifenstein, A. Marx, R. Gross, and S. T. B. Goennenwein, "High cooperativity in coupled microwave resonator ferrimagnetic insulator hybrids," Phys. Rev. Lett. **111**, 127003 (2013).
[5]M. Goryachev, W. G. Farr, D. L. Creedon, Y. Fan, M. Kostylev, and M. E. Tobar, "High-cooperativity cavity QED with magnons at microwave frequencies," Phys. Rev. Appl. **2**, 054002 (2014).
[6]Y. Tabuchi, S. Ishino, T. Ishikawa, R. Yamazaki, K. Usami, and Y. Nakamura, "Hybridizing ferromagnetic magnons and microwave photons in the quantum limit," Phys. Rev. Lett. **113**, 083603 (2014).
[7]X. Zhang, C.-L. Zou, L. Jiang, and H. X. Tang, "Strongly coupled magnons and cavity microwave photons," Phys. Rev. Lett. **113**, 156401 (2014).
[8]A. Osada, R. Hisatomi, A. Noguchi, Y. Tabuchi, R. Yamazaki, K. Usami, M. Sadgrove, R. Yalla, M. Nomura, and Y. Nakamura, "Cavity optomagnonics with spin-orbit coupled photons," Phys. Rev. Lett. **116**, 223601 (2016).
[9]X. Zhang, N. Zhu, C.-L. Zou, and H. X. Tang, "Optomagnonic whispering gallery microresonators," Phys. Rev. Lett. **117**, 123605 (2016).
[10]J. Haigh, A. Nunnenkamp, A. Ramsay, and A. Ferguson, "Triple-resonant Brillouin light scattering in magneto-optical cavities," Phys. Rev. Lett. **117**, 133602 (2016).
[11]X. Zhang, C.-L. Zou, L. Jiang, and H. X. Tang, "Cavity magnomechanics," Sci. Adv. **2**, e1501286 (2016).
[12]J. Li, S.-Y. Zhu, and G. Agarwal, "Magnon-photon-phonon entanglement in cavity magnomechanics," Phys. Rev. Lett. **121**, 203601 (2018).
[13]H. Xiong, "Center-of-mass magnomechanics beyond magnetostrictive limits," Sci. China: Phys., Mech. Astron. **68**, 250313 (2025).
[14]Y. Tabuchi, S. Ishino, A. Noguchi, T. Ishikawa, R. Yamazaki, K. Usami, and Y. Nakamura, "Coherent coupling between a ferromagnetic magnon and a superconducting qubit," Science **349**, 405–408 (2015).
[15]D. Lachance-Quirion, S. P. Wolski, Y. Tabuchi, S. Kono, K. Usami, and Y. Nakamura, "Entanglement-based single-shot detection of a single magnon with a superconducting qubit," Science **367**, 425–428 (2020).
[16]B. Wang, X.-H. Lu, X. Jia, and H. Xiong, "Coherent stimulated amplification of the skyrmion breathing," Chaos Soliton. Fract. **171**, 113484 (2023).
[17]X.-F. Pan, P.-B. Li, X.-L. Hei, X. Zhang, M. Mochizuki, F.-L. Li, and F. Nori, "Magnon-skyrmion hybrid quantum systems: Tailoring interactions via magnons," Phys. Rev. Lett. **132**, 193601 (2024).
[18]D. Xu, X.-K. Gu, H.-K. Li, Y.-C. Weng, Y.-P. Wang, J. Li, H. Wang, S.-Y. Zhu, and J. You, "Quantum control of a single magnon in a macroscopic spin system," Phys. Rev. Lett. **130**, 193603 (2023).
[19]A. Kani, B. Sarma, and J. Twamley, "Intensive cavity-magnomechanical cooling of a levitated macromagnet," Phys. Rev. Lett. **128**, 013602 (2022).
[20]M. Asjad, J. Li, S.-Y. Zhu, and J. You, "Magnon squeezing enhanced ground-state cooling in cavity magnomechanics," Fundam. Res. **3**, 3–7 (2023).
[21]X. Zhang, C.-L. Zou, N. Zhu, F. Marquardt, L. Jiang, and H. X. Tang, "Magnon dark modes and gradient memory," Nat. Commun. **6**, 8914 (2015).
[22]R. Hisatomi, A. Osada, Y. Tabuchi, T. Ishikawa, A. Noguchi, R. Yamazaki, K. Usami, and Y. Nakamura, "Bidirectional conversion between microwave and light via ferromagnetic magnons," Phys. Rev. B **93**, 174427 (2016).
[23]B. Wang, Z.-X. Liu, C. Kong, H. Xiong, and Y. Wu, "Magnon-induced transparency and amplification in PT-symmetric cavity-magnon system," Opt. Express **26**, 20248–20257 (2018).
[24]F. Wang and C. Gou, "Magnon-induced absorption via quantum interference," Opt. Lett. **48**, 1164–1167 (2023).
[25]C. Kong, B. Wang, Z.-X. Liu, H. Xiong, and Y. Wu, "Magnetically controllable slow light based on magnetostrictive forces," Opt. Express **27**, 5544–5556 (2019).
[26]Y.-P. Wang, G.-Q. Zhang, D. Zhang, X.-Q. Luo, W. Xiong, S.-P. Wang, T.-F. Li, C.-M. Hu, and J. Q. You, "Magnon Kerr effect in a strongly coupled cavity-magnon system," Phys. Rev. B **94**, 224410 (2016).
[27]G. Zhang, Y. Wang, and J. You, "Theory of the magnon Kerr effect in cavity magnonics," Sci. China: Phys., Mech. Astron. **62**, 987511 (2019).
[28]Y.-P. Wang, G.-Q. Zhang, D. Zhang, T.-F. Li, C.-M. Hu, and J. You, "Bistability of cavity magnon polaritons," Phys. Rev. Lett. **120**, 057202 (2018).
[29]R.-C. Shen, J. Li, Z.-Y. Fan, Y.-P. Wang, and J. You, "Mechanical bistability in Kerr-modified cavity magnomechanics," Phys. Rev. Lett. **129**, 123601 (2022).
[30]M. Kumar Singh, S. Mahajan, V. Bhatt, S. Yadav, P. K. Jha, and A. B. Bhattacherjee, "Tunable bistability, optomechanical and magnomechanically induced transparency in opto-magnomechanical system," J. Appl. Phys. **136**, 214401 (2024).
[31]Z.-X. Liu, B. Wang, H. Xiong, and Y. Wu, "Magnon-induced high-order sideband generation," Opt. Lett. **43**, 3698–3701 (2018).
[32]W.-L. Xu, Y.-P. Gao, T.-J. Wang, and C. Wang, "Magnon-induced optical high-order sideband generation in hybrid atom-cavity optomagnonical system," Opt. Express **28**, 22334–22344 (2020).
[33]W. Liu, Y. Zhang, Z. Deng, J. Ye, K. Wang, B. Wang, D. Gao, and P. Lu, "On-chip chiral mode switching by encircling an exceptional point in an anti-parity-time symmetric system," Laser Photonics Rev. **16**, 2100675 (2022).
[34]Y.-H. Lai, Y.-K. Lu, M.-G. Suh, Z. Yuan, and K. Vahala, "Observation of the exceptional-point-enhanced Sagnac effect," Nature **576**, 65–69 (2019).
[35]Y.-P. Wang and C.-M. Hu, "Dissipative couplings in cavity magnonics," J. Appl. Phys. **127**, 130901 (2020).
[36]M. Harder, Y. Yang, B. Yao, C. Yu, J. Rao, Y. Gui, R. Stamps, and C.-M. Hu, "Level attraction due to dissipative magnon-photon coupling," Phys. Rev. Lett. **121**, 137203 (2018).
[37]P.-C. Xu, J. W. Rao, Y. S. Gui, X. Jin, and C.-M. Hu, "Cavity-mediated dissipative coupling of distant magnetic moments: Theory and experiment," Phys. Rev. B **100**, 094415 (2019).
[38]V. L. Grigoryan and K. Xia, "Cavity-mediated dissipative spin-spin coupling," Phys. Rev. B **100**, 014415 (2019).
[39]J. Zhao, Y. Liu, L. Wu, C.-K. Duan, Y.-X. Liu, and J. Du, "Observation of anti-PT-symmetry phase transition in the magnon-cavity-magnon coupled system," Phys. Rev. Appl. **13**, 014053 (2020).

[40]Y.-P. Wang, J. Rao, Y. Yang, P.-C. Xu, Y. Gui, B. Yao, J. You, and C.-M. Hu, "Nonreciprocity and unidirectional invisibility in cavity magnonics," Phys. Rev. Lett. **123**, 127202 (2019).
[41]J. Qian, J. W. Rao, Y. S. Gui, Y. P. Wang, Z. H. An, and C.-M. Hu, "Manipulation of the zero-damping conditions and unidirectional invisibility in cavity magnonics," Appl. Phys. Lett. **116**, 192401 (2020).
[42]M. Kim, A. Tabesh, T. Zegray, S. Barzanjeh, and C.-M. Hu, "Nonreciprocity in cavity magnonics at millikelvin temperature," J. Appl. Phys. **135**, 063904 (2024).
[43]Y. Wang, W. Xiong, Z. Xu, G.-Q. Zhang, and J.-Q. You, "Dissipation-induced nonreciprocal magnon blockade in a magnon-based hybrid system," Sci. China: Phys., Mech. Astron. **65**, 260314 (2022).
[44]R. Lü, H. Zhan, D. Kong, and F. Wang, "Dissipation-induced nonreciprocal magnon entanglement and one-way steering in waveguide electromagnonics," Opt. Lett. **49**, 7032–7035 (2024).
[45]J. M. Nair, D. Mukhopadhyay, and G. Agarwal, "Enhanced sensing of weak anharmonicities through coherences in dissipatively coupled anti-PT symmetric systems," Phys. Rev. Lett. **126**, 180401 (2021).
[46]T.-X. Lu, H. Zhang, Q. Zhang, and H. Jing, "Exceptional-point-engineered cavity magnomechanics," Phys. Rev. A **103**, 063708 (2021).
[47]T. Wang, W. Zhang, J. Cao, and H.-F. Wang, "Exceptional-point-engineered phonon laser in a cavity magnomechanical system," New J. Phys. **25**, 083045 (2023).
[48]Y. Yang, Y.-P. Wang, J. Rao, Y. Gui, B. Yao, W. Lu, and C.-M. Hu, "Unconventional singularity in anti-parity-time symmetric cavity magnonics," Phys. Rev. Lett. **125**, 147202 (2020).
[49]J. M. P. Nair, D. Mukhopadhyay, and G. S. Agarwal, "Ultralow threshold bistability and generation of long-lived mode in a dissipatively coupled nonlinear system: Application to magnonics," Phys. Rev. B **103**, 224401 (2021).
[50]H. Pan, Y. Yang, Z. H. An, and C.-M. Hu, "Bistability in dissipatively coupled cavity magnonics," Phys. Rev. B **106**, 054425 (2022).
[51]C. Zhao, Z. Yang, R. Peng, J. Yang, C. Li, and L. Zhou, "Dissipative-coupling-induced transparency and high-order sidebands with Kerr nonlinearity in a cavity-magnonics system," Phys. Rev. Appl. **18**, 044074 (2022).
[52]H. Xiong, L.-G. Si, A.-S. Zheng, X. Yang, and Y. Wu, "Higher-order sidebands in optomechanically induced transparency," Phys. Rev. A **86**, 013815 (2012).
[53]M.-A. Lemonde, N. Didier, and A. A. Clerk, "Nonlinear interaction effects in a strongly driven optomechanical cavity," Phys. Rev. Lett. **111**, 053602 (2013).
[54]A. Kronwald and F. Marquardt, "Optomechanically induced transparency in the nonlinear quantum regime," Phys. Rev. Lett. **111**, 133601 (2013).
[55]S. Liu, W.-X. Yang, Z. Zhu, T. Shui, and L. Li, "Quadrature squeezing of a higher-order sideband spectrum in cavity optomechanics," Opt. Lett. **43**, 9–12 (2018).
[56]S.-N. Huai, Y.-L. Liu, J. Zhang, L. Yang, and Y.-X. Liu, "Enhanced sideband responses in a PT-symmetric-like cavity magnomechanical system," Phys. Rev. A **99**, 043803 (2019).
[57]T.-X. Lu, X. Xiao, L.-S. Chen, Q. Zhang, and H. Jing, "Magnon-squeezing-enhanced slow light and second-order sideband in cavity magnomechanics," Phys. Rev. A **107**, 063714 (2023).
[58]A. Wahab, M. Abbas, X. Yang, and Y. Chen, "Generation of second-order sidebands and slow-fast light in cavity magnomechanics with a parametric amplifier," Chaos Soliton. Fract. **187**, 115436 (2024).
[59]S. Weis, R. Rivière, S. Deléglise, E. Gavartin, O. Arcizet, A. Schliesser, and T. J. Kippenberg, "Optomechanically induced transparency," Science **330**, 1520–1523 (2010).
[60]S. Bayati, M. Bagheri Harouni, and A. Mahdifar, "Magnomechanically induced transparency and tunable slow-fast light via a levitated micromagnet," Opt. Express **32**, 14914–14928 (2024).
[61]B. Chen, L. Shang, X.-F. Wang, J.-B. Chen, H.-B. Xue, X. Liu, and J. Zhang, "Atom-assisted second-order sideband generation in an optomechanical system with atom-cavity-resonator coupling," Phys. Rev. A **99**, 063810 (2019).
[62]X. Xiao, Q. Liao, N. Zhou, W. Nie, and Y. Liu, "Tunable optical second-order sideband effects in a parity-time symmetric optomechanical system," Sci. China: Phys., Mech. Astron. **63**, 114211 (2020).
[63]Y.-F. Jiao, T.-X. Lu, and H. Jing, "Optomechanical second-order sidebands and group delays in a Kerr resonator," Phys. Rev. A **97**, 013843 (2018).
[64]J. Li, J. Li, Q. Xiao, and Y. Wu, "Giant enhancement of optical high-order sideband generation and their control in a dimer of two cavities with gain and loss," Phys. Rev. A **93**, 063814 (2016).
[65]Y. Jiao, H. Lü, J. Qian, Y. Li, and H. Jing, "Nonlinear optomechanics with gain and loss: Amplifying higher-order sideband and group delay," New J. Phys. **18**, 083034 (2016).
[66]Q. Liao, M. Song, and W. Bao, "Generation of second-order sideband and slow-fast light effects in a PT-symmetric optomechanical system," Chaos Soliton. Fract. **166**, 112978 (2023).
[67]W.-X. Yang, A.-X. Chen, X.-T. Xie, and L. Ni, "Enhanced generation of higher-order sidebands in a single-quantum-dot-cavity system coupled to a PT-symmetric double cavity," Phys. Rev. A **96**, 013802 (2017).
[68]T.-X. Lu, Z.-S. Li, B. Yin, J. Wang, X. Xiao, and H. Jing, "Magnetic-field-direction-controlled slow light and second-order sidebands in a cavity-magnon optomechanical system," Opt. Express **32**, 48302–48314 (2024).
[69]W.-A. Li, G.-Y. Huang, J.-P. Chen, and Y. Chen, "Nonreciprocal enhancement of optomechanical second-order sidebands in a spinning resonator," Phys. Rev. A **102**, 033526 (2020).
[70]X. Wang, K.-W. Huang, and H. Xiong, "Nonreciprocal sideband responses in a spinning microwave magnomechanical system," Opt. Express **31**, 5492–5506 (2023).
[71]M. Wang, C. Kong, Z.-Y. Sun, D. Zhang, Y.-Y. Wu, and L.-L. Zheng, "Nonreciprocal high-order sidebands induced by magnon Kerr nonlinearity," Phys. Rev. A **104**, 033708 (2021).
[72]C. Wang, J. Rao, Z. Chen, K. Zhao, L. Sun, B. Yao, T. Yu, Y.-P. Wang, and W. Lu, "Enhancement of magnonic frequency combs by exceptional points," Nat. Phys. **20**, 1139–1144 (2024).
[73]X. Huang, C. Lu, C. Liang, H. Tao, and Y.-C. Liu, "Loss-induced nonreciprocity," Light: Sci. Appl. **10**, 30 (2021).
[74]X. Huang and Y.-C. Liu, "Perfect nonreciprocity by loss engineering," Phys. Rev. A **107**, 023703 (2023).
[75]B. Li, Y. Zuo, L.-M. Kuang, H. Jing, and C. Lee, "Loss-induced quantum nonreciprocity," npj Quantum Inf. **10**, 75 (2024).
[76]B. Yao, T. Yu, X. Zhang, W. Lu, Y. Gui, C.-M. Hu, and Y. M. Blanter, "The microscopic origin of magnon-photon level attraction by traveling waves: Theory and experiment," Phys. Rev. B **100**, 214426 (2019).
[77]Y. Zhao, J. Rao, Y. Gui, Y. Wang, and C.-M. Hu, "Broadband nonreciprocity realized by locally controlling the Magnon's radiation," Phys. Rev. Appl. **14**, 014035 (2020).
[78]Z.-X. Liu, "Dissipative coupling induced UWB magnonic frequency comb generation," Appl. Phys. Lett. **124**, 032403 (2024).
[79]L.-J. Cong, Y.-X. Luo, Z.-P. Cheng, R.-B. Du, H.-Y. Liu, R.-C. Yang, and Y. Ming, "Chirally-symmetric-like unconventional magnon blockade in a dissipative cavity-magnon system," Results Phys. **66**, 108023 (2024).
[80]J. Yang, C. Zhao, D.-W. Wang, R. Peng, and L. Zhou, "Dissipative-coupling-induced steady-state entanglement and one-way steering in a cavity-magnonics system," Phys. Rev. Appl. **21**, 044056 (2024).